electronics

MDPI

Article

Synthesis of Rectenna for Powering Micro-Watt Sensors by Harvesting Ambient RF Signals' Power

Apostolia Karampatea and Katherine Siakavara *

Radiocommunications Lab and School of Physics, Aristotle University of Thessaloniki, Thessaloniki 54124, Greece; akarampa@physics.auth.gr

* Correspondence: skv@auth.gr

Received: 12 August 2019; Accepted: 30 September 2019; Published: 1 October 2019

Abstract: In the article, a dual and wide band antenna array suitable for RF rectenna applications was synthesized and global rectenna systems are presented. The array consists of two bowtie-shaped patches, printed on the one side of a dielectric slab (FR4). On the other side of the slab, an aperture-textured metallic ground layer, is printed. Examples of full-wave rectifiers connected, through matching networks, to the antenna elements and forming integrated rectenna systems for radio-frequency (RF) power harvesting at 868 MHz, from 920 to 960 MHz and at 1.8 GHz, are presented. Statistical results over frequency and the directions of arrival (DoAs) of incoming waves were received showing, at the rectifier, mean direct current (DC) voltage of 580 mV, and mean power of 58 μW, for circularly polarized waves of field intensity of 1.8 V/m. The DC voltage can reach 800 mV, the power 120 μW and the efficiency 68% when the waves come from DoAs of maximum antenna's gain. Due to the wideband performance of the antenna, it could be used at various frequency slots as long as the matching network's operation frequency is changed. Thus the proposed rectennas could be suitable for energizing low-power sensors or at least to charge their batteries.

Keywords: rectenna; dual band antennas; bowtie antennas; ambient RF power harvesting

1. Introduction

Nowadays and in the near future, low-power wireless electrical and electronic sensors are expected to play an important role and provide support to the infrastructure of the rapidly developing web of Internet of Things (IoT). The almost ubiquitous presence of such sensors, which will permit the wireless connection of access points of the web, serving various human and machine activities, entails the operation of a huge number of sensors and the problem of powering them arises. The ordinary solution of this problem is the utilization of batteries. However, due to the large number of sensors in combination with the peculiarity of modern networks, which would potentially require the presence of sensors in confined spaces or remote locations, the use of batteries, which have limited lifetime and require periodical maintenance, could not be practical. Recently the utilization of the power of electromagnetic waves (EWs), which permanently exist in the environment, has gained attention as a promising electric power resource suitable for low-power sensors. The basic idea is the exploitation of the great number of radio-frequency (RF) power systems, which radiate EWs, such as wireless local area network (WLAN) routers, cellular network base stations and TV and radio broadcasting towers [1]. The ambient EW power, emanated by these sources, spreads over more than one frequency bands which extend from the ultra-high frequency (UHF) range, as with the TV and radio stations, to more than 5 GHz, including the 900 MHz band, the long-range (LoRA) spread spectrum modulation technique for long-range transmissions system at 868 MHz, the DCS 1800 MHz, the Universal Mobile Telecommunication System (UMTS) around 2 GHz, the well known Industrial, Scientific and Medical (ISM) band at 2.4 GHz, etc. The energy available in these different bands may be harvested by using

appropriate antennas. As the ambient electromagnetic energy can be continuously harvested, and in turn be converted, by rectification, to direct current (DC) power and also be stored, it grows to be an effective way to ensure the powering of the sensors, either making them energy autonomous or extending their batteries' lifetime. These ideas and process, known as wireless energy harvesting (WEH), although not new, continue to evolve and to be demanded in many applications. An advanced step to this technology would be not only the scavenging of the existing ambient electromagnetic power but the powering of the sensors, directly and wirelessly, by electromagnetic power-radiating systems which operate exclusively for this purpose, termed as far-field wireless power transfer (WPT) systems. For example, it would be not difficult to create a radiating system supplied by an antenna having a radiation pattern with a main beam directed towards an area inside which wireless sensors are interspersed, each one of which is supplied by its own antenna that would catch this energy. Whatever is the source of the EWs impinging to a sensor, in order for the RF energy be harvested, the sensor must be supplied by a suitable antenna and a rectifier to convert the RF to DC power. Thus the antenna and the rectifier are the basic units of a harvesting system, giving to it the name 'rectenna'. However, they are insufficient as an additional unit for the maximum energy transfer from the antenna to the rectifier, ensuring the effective operation of the rectenna, along with a unit for storing the DC power are necessary. In conclusion, the optimal design of a global rectenna system is a challenge for the designer.

The appropriate design of receiving antennas intended for rectennas is very important since their characteristics as their gain, their radiation efficiency and generally the multi- or wide- frequency band operation affect the amount of harvested energy. Many types of rectennas with satisfactory conversion efficiency have been developed and are supplied with different types of antennas, the more popular of them being patch antennas of various layouts. In [2], patch antennas, of shapes modified with intend maximum radiation efficiency and small size to be obtained are proposed as good candidates for rectenna synthesis at 2.45 GHz. In [3] a simple printed antenna of dipole type with high efficiency is proposed. The antenna is designed with incorporated elements which ensure directly conjugate match to the rectifier at 2.45 GHz. The maximum obtained conversion efficiency is 83% and smaller values are achieved for low input power level, however, remaining larger than 50%. In the rectennas of [4] two different rectification topologies for maximum RF-to-DC power conversion efficiency are proposed. The used antenna is a 2×2 array of miniaturized printed patches and conversion efficiency up to 70% is obtained. The rectenna designed in [5], has dual band operation, at 915 MHz and 2.45 GHz, and consists of a slot-loaded dual-band folded dipole antenna of small size and a dual-band rectifier. The obtained conversion efficiency is 37% and 30% at the low and high band, respectively. Paper [6] introduces an interesting ultra-lightweight multiband RF energy rectenna, fabricated on paper substrate. It is designed to operate in all Long Term Evolution(LTE) frequency bands. The entire system is compact, integrating antenna and rectifier and the obtained RF-to-DC conversion efficiency in the range of 5–16% for an available input power of −20 dBm in all bands, and the conversion increases up to 30% when this power reaches −15 dBm. In [7], a rectenna with antenna of slot dipole type was designed for use at 2.45 GHz with conversion efficieny ~59.5%. In [8], a rectenna system was designed with an antenna of stacked orthogonal patches and also parasitic elements for matching and increase of gain reasons. The conversion efficiency obtained is 20%. In [9], a dual-port triple-band microstrip patch rectenna, with efficiency greater than 40% for ambient RF energy harvesting using the GSM-900, GSM-1800, and UMTS-2100 bands, is proposed. Its antenna is implemented by stacking two single-port patch antennas back to back. Each port can independently harvest the RF signal from a half-space with high gain and the antenna can harvest RF energy from almost all directions. An output voltage of more than 600 mV is obtained, when the power density is greater than 500 $\mu W/m^2$.

In [10,11] meander-type monopoles or folded dipoles are proposed for synthesis of rectennas with efficiency exceeding 20%. In [12] an efficient antenna based on the traditional straight and planar half-wavelength dipole, which by suitable geometrical modification resulted in a radiator of quasi-circular shape with increased frequency bandwidth and operation at 868 MHz/915 MHz. The antenna incorporated with rectifying circuit obtains RF-to-DC conversion efficiency, which reaches

at 37%. In [13] a rectenna provided with an antenna of printed strip dipoles with partial ground plane and an adaptive stub for matching to the rectifier at 5.2 and 5.8 GHz is proposed. The rectenna exhibits conversion efficiency which exceeds the level of 50%. In [14] two antenna structures, one of quatrefoil shape CPW-Fed monopole configuration and the other of quatrefoil slot antenna layout which obtain radiation efficiency exceeding 91% are proposed as potential radiating systems, suitable for rectenna devices.

Moreover, antennas composed of arrays of discrete elements or elements interconnected and forming a grid arrangement, seem to contribute to the efficient operation of rectennas. In [15] the antenna array topology of five cells each one consisting of a quasi-Yagi dipole antenna with variable numbers of interconnected directors is proposed and a rectenna with multidirectional receiving capabilities is produced at 2.45 GHz. In [16], a two port grid-array antenna which operates as travelling wave radiator is synthesized at 2.45 GHz and combined with coplanar stripline-based rectifier constitutes a global rectenna device with RF to DC conversion efficiency of 16.3–45.3% depending on the level of the harvested power. In [17] a novel four-cascaded element array of orthogonal patches, with a series fed two by two, is proposed for the synthesis of a rectenna device at 2.45 GHz. The rectenna exhibits a maximum RF to DC conversion efficiency of 77.2%. In [18], a multiport rectenna for ambient radio-frequency (RF) energy harvesting, consisting of an optimized triple-port pixel antenna and a triple-port rectifier with DC combining, is proposed. Its multiport pixel structure leads to enhanced harvested RF power for a given area as well as to reduction in the antenna matching requirements. The overall RF-to-DC efficiency of the rectenna is shown to be 19% when the total input RF power is −20 dBm.

In [19,20], prototypes of wire dipoles and of printed dipole configurations, incorporated to novel double negative (DNG) dielectric substrates for the increase of the amount of the harvested energy, are proposed.

Antennas of bowtie configuration, either as wire frame or as printed patches, have also been proposed for rectenna synthesis. In [21,22], printed wide band antenna elements with shape based on the traditional bowtie layout but reconfigured and powered by properly designed feeding systems and mechanisms, were designed and proposed. While, in [23] grids of bowtie antenna elements connected with diodes and operating as efficient rectenna devices, were designed at 2.45 GHz and at 5 GHz.

It is worthwhile mentioning that in parallel with the merits of the presence of RF ambient signals there is a demerit too. Their power levels are small compared to those of other ambient energy resources such as the solar power, the wind or the vibration power. Indicatively, in a typical urban area, the RF power density is about 0.2 nW/cm^2–1 μW/cm^2 [24] and also these levels do not remain constant due, for example, to the multipath effects. Consequently the achieved DC power after the conversion from AC to DC is small and also not constant. A promising solution to this problem, taking in parallel into account that the frequencies of ambient RF sources are spread over a wide part of the electromagnetic spectrum could be the utilization of multi- or wide-band rectennas. Such systems could accumulate more energy from different frequency channels simultaneously, and in this way could produce a DC output power of satisfactory levels. Thus several papers are focused on the design of dual or multi-band antennas for the synthesis of RF harvesters, as previously was mentioned.

The target of the present work was the synthesis of an antenna suitable for effective RF energy scavenging within a range including the upper part of the UHF band and exceeding the frequency of 2 GHz. Consequently, the antenna might have wideband characteristics. Also, at most of the applications, it is preferable for the rectennas to have low weight and profile. Moreover, the rectennas harvest power from RF waves propagating in a built environment and due to the multipath phenomenon, the DoAs of the waves are random. So, the rectenna's antenna has to effectively gather RF power from a portion of the surrounding space as large as possible. Due to these required technical specifications, in the present work the patch-type antenna was selected and the basic configuration used was that of a bowtie by which it is well known that wide band operation could be obtained. However, extensive reconfiguration was made in order for two and simultaneously wideband frequency operations to be

obtained. The final layout of the entire antenna is a semi-printed antenna array of two bowties with specifically textured ground plane which permits the entire system to receive signals effectively from both, the front and the back side of the antenna. Moreover, with the intention to operate effectively in the upper part of the UHF range, its physical size is expected be relatively large. For this purpose and for saving space, the use of two bowtie elements incorporated in the same ground frame was selected. By this selection, the gathered power would increase without the size of the antenna to increase too.

2. The Designed Rectenna and Its Performance

The first step of the synthesis of the rectenna was the design of its antenna with one element of bowtie shape (Antenna_1). Then, using this antenna configuration, the design of a two bowtie element array (Antenna_2) was made.

2.1. Antenna_1

The classical way to design a bowtie antenna of microstrip type, shown in Figure 1, is to find its geometrical parameters using, for example, the approximate mathematical formula [25]:

$$f_r = 1.152\frac{c}{L^2\sqrt{\varepsilon_{eff}}}\left(\frac{(W+2\Delta L)+(W_c+2\Delta L)}{(W+2\Delta L)(S+2\Delta L)}\right)^{-1} \quad (1)$$

where, f_r is the frequency of resonance the parameters W, S, L and W_c are shown in Figure 1, and ΔL, ε_{eff} are defined as

$$\Delta L = \frac{0.412h(\varepsilon_{eff}+0.3)\left(\frac{W+W_c}{2h}+0.262\right)}{\left[(\varepsilon_{eff}-0.258)\left(\frac{W+W_c}{2h}+0.813\right)\right]} \quad \text{and} \quad \varepsilon_{eff} = \left(\frac{\varepsilon_r+1}{2}\right)+\left(\frac{\varepsilon_r-1}{2}\right)\left(\frac{24h}{W+W_c}+1\right)^{-1/2}$$

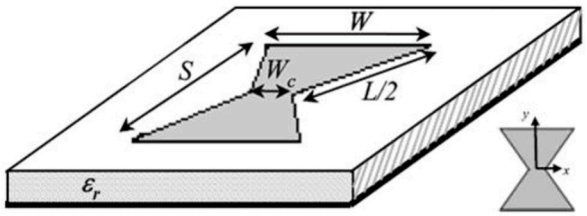

Figure 1. The layout of an ordinary microstrip bowtie antenna.

Equation (1) shows that f_r depends on W, W_c, L and S, and, by study, it is ascertained that there are more than one sets of these parameters' values which provide the same f_r. So, a parametric study could precede the design of a bowtie microstrip element and then selection of the proper set of values could be made. However, the final parameter values are found via repeated simulations and would potentially be different from those found by the above equations.

The microstip character of this antenna, due to the cavity with open walls, formed between the metallic planar bowtie patch and the ground plane, leads to very narrow frequency band of operation and effective radiation or receipt of waves appears only towards or from the half space in front of the antenna. This performance is valid for all the microstrip antennas but is not desirable for a rectenna. So, in the present work, the initial antenna configuration was a microstrip bowtie with compact ground plane (as in Figure 1) and then the ground plane was properly textured. In detail, a large aperture was created with the intention to permit the bowtie patch to operate as a printed radiating element, thus enhancing the width of its frequency band of operation and simultaneously permitting the antenna to receive signals from both half spaces, in the front of and back of its plane. Besides the texturing of the ground plane, the values of the geometrical parameters of the bowtie were differentiated from those produced by Equation (1). The entire process was carried out via repeated simulations of the antenna's

operation by an electromagnetic solver (CST). The modifications made at the layout of the antenna during the iterations, were focusing to make it work in two frequency bands, of large width and also the antenna's input impedance to have values that could be easily matched to the rectifier. The lower band had to cover a part of the upper UHF band and exceeding the frequency of 1 GHz and the higher one, to cover a range before 2 GHz and also exceeding this frequency. The dominant parameter for control of the characteristics of operation in the low-frequency band was the size, the geometry and generally the texturing of the ground plane while control within the high band was obtained via the values of the bowtie's geometrical parameters. The entire antenna could be characterized as hybrid or perhaps as semi-printed radiator because ground plane exists but it is compact only behind the feeding lines, supporting the Transverse Electric and Magnetic (TEM)mode of the feeding signal, while the bowtie patches are not substantially of microstrip type but of just printed type, as behind them there is not ground.

The final layout of the synthesized antenna, Antenna_1, is depicted in Figure 2. It includes the bowtie patch which is printed, via copper, on dielectric substrate FR4, with ε_r = 4.4, thickness h = 1.6 mm and loss tangent considered to be ~0.015 in the entire frequency band of calculations, taking into account that the thickness of the copper ground layer and of the bowtie patch is 0.07 mm the entire thickness of the antenna is 1.74 mm. The patch is fed by microstrip line with characteristic impedance 50 Ω through a wider line of width d, for matching purpose. The antenna's geometrical parameter values are included in Table 1.

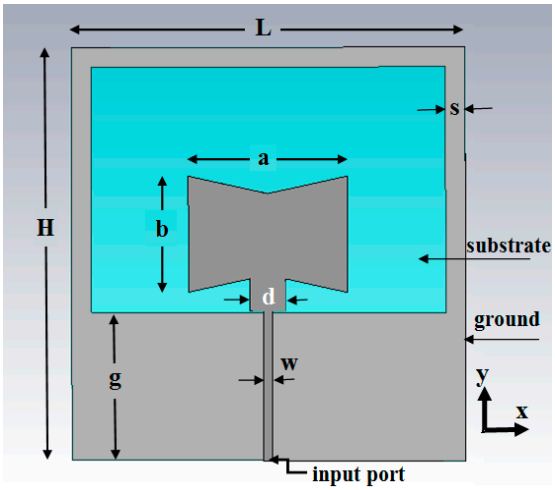

Figure 2. The layout of Antenna_1.

Table 1. Geometrical parameter values of Antenna_1 in [mm].

L	H	a	b	d	g	w	s
132	138.6	53.25	38.95	10.67	50.40	3	6.60

The performance of Antenna_1 is shown in Figures 3 and 4. Figure 3a depicts the real and imaginary part of the antenna's input impedance, Z_{in}. Figure 3b presents the scattering coefficient of the feeding signal at the antenna's input and shows the two bands inside which $S_{11} < -10$dB, considering port impedance 50 Ω. The low band extends from 0.75 GHz to 1.25 GHz, so the bandwidth (BW) is 50%. The high band extends from 1.63 GHz to 2.31 GHz and the BW is 34.5%.

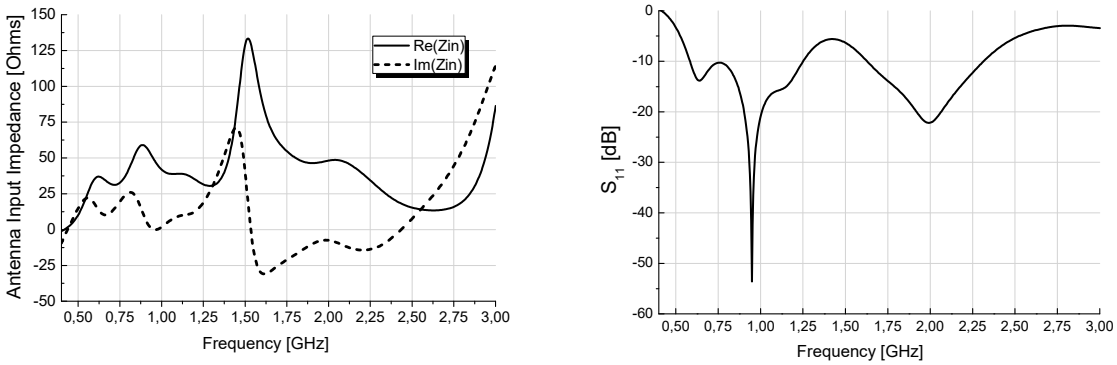

(**a**) (**b**)

Figure 3. Antenna_1: (**a**) real and imaginary part of the antenna's input impedance, (**b**) scattering coefficient of the feeding signal at the input of the antenna.

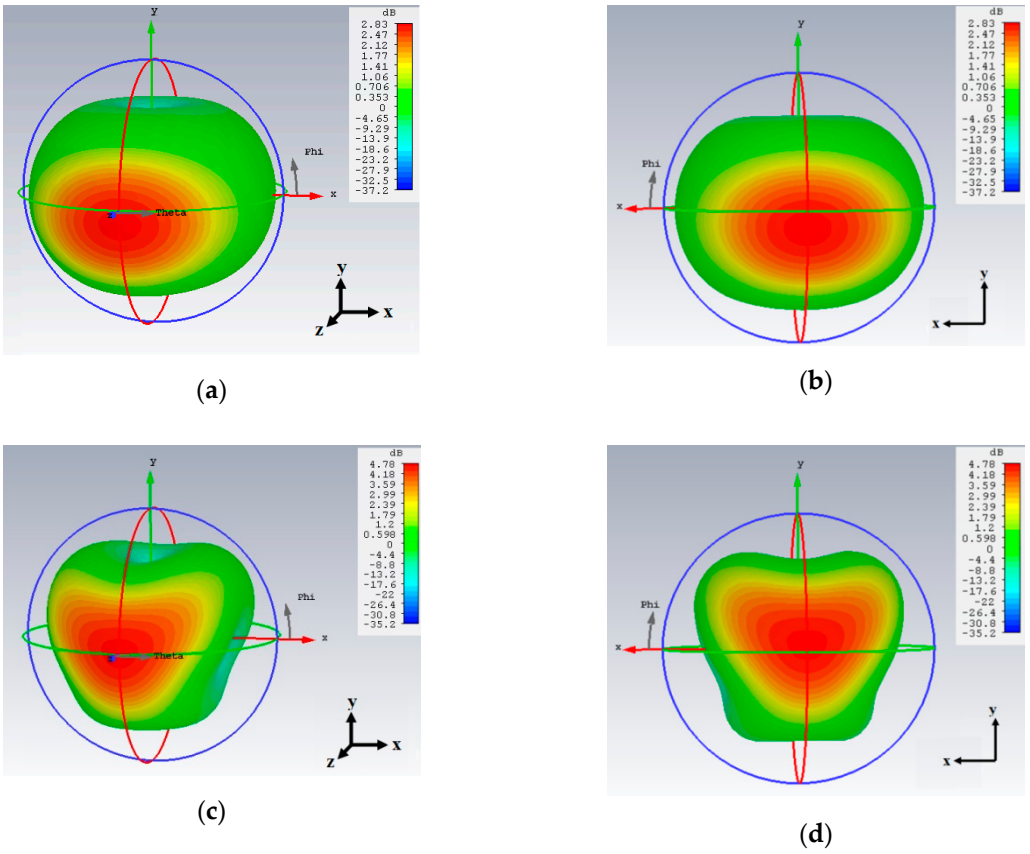

(**a**) (**b**)

(**c**) (**d**)

Figure 4. 3D realized gain patterns of Antenna_1: At 868 MHz, views from (**a**) in front of the antenna's plane and (**b**) at the back of the antenna. At 1.8 GHz, (**c**) in front of and (**d**) at the back of the antenna.

Figure 4 illustrates the 3D gain patterns of the antenna at the low band, indicatively at 0.868 GHz and in the high band e.g., at 1.8 GHz. Levels of maximum gain, near to 2.8 dB at the low and 4.8 dB at the high band, are obtained. It is shown that the antenna radiates and consequently receives signals with satisfactory high-gain values from both half spaces, in the front and back of the antenna's plane. This performance is especially desired in case of ambient energy harvesting.

2.2. *Antenna_2*

Given the satisfactory performance of the Antenna_1, its configuration was used for the synthesis of a two similar element array (Antenna_2). Its layout is depicted in Figure 5. The entire -xy- dimensions

of the ground frame and of the dielectric were made a little larger than those of Antenna_1, in order for there to be room for the two bowties, and generally all the geometrical parameters of bowties, feeding lines, ground plane and dielectric were changed with the intention of each bowtie to hold, as far as possible, its operational features. The new values of the geometrical parameters are included in Table 2 and were found via repeated simulations.

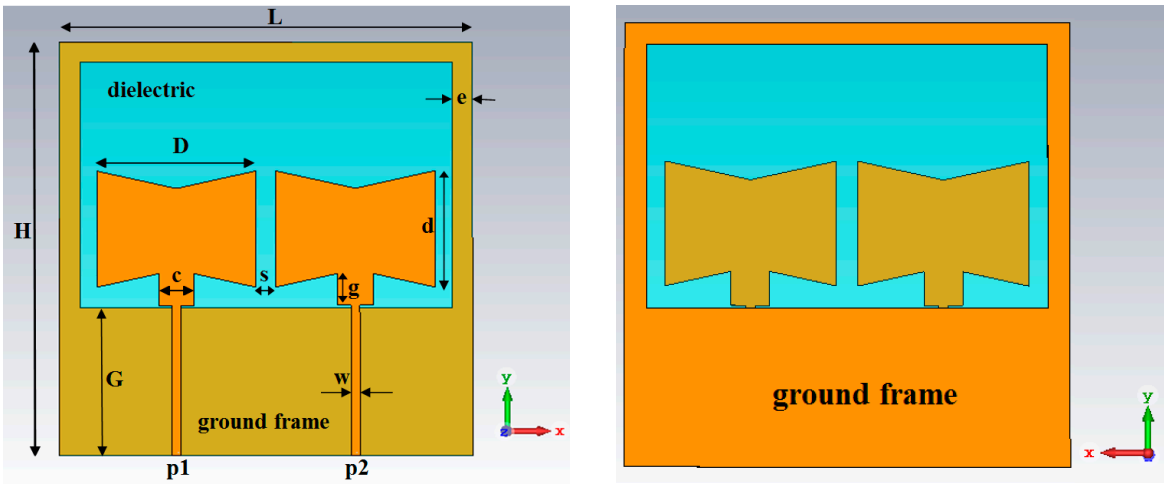

(**a**) (**b**)

Figure 5. The layout of Antenna_2: (**a**) front side (**b**) back side.

Table 2. Geometrical paremeter values of Antenna_2 in [mm].

L	H	G	D	s	d	g	c	w	e
138.60	138.60	49.50	53.20	6.78	38.95	18.71	12	3	7

The input impedances at the feeding ports p1 and p2 are of equal value, due to the similarity of the bowties and their symmetrical placement with respect to the ground frame, and are illustrated in Figure 6a. In the values of the presented impedances the mutual coupling between the bowtie elements has been taken into account.

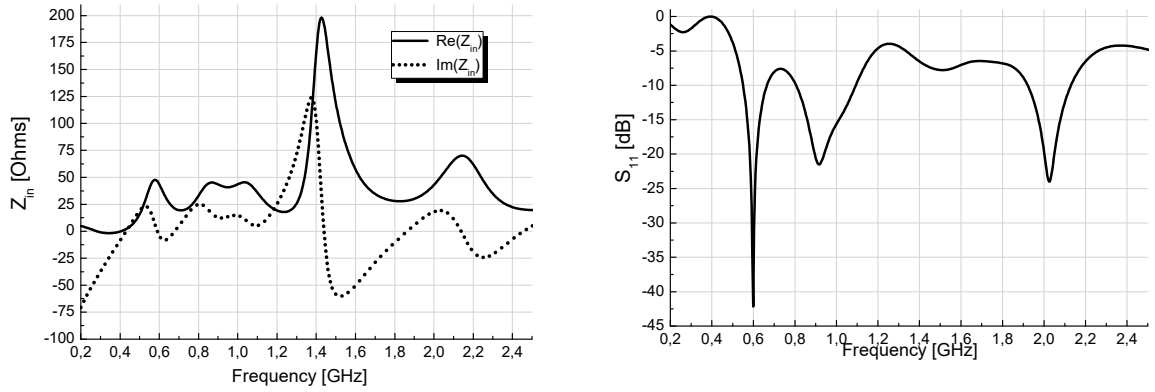

(a) (b)

Figure 6. Antenna_2: (**a**) real and imaginary parts of the input impedances of its similar elements, (**b**) signal scattering coefficient at each element's input considering a 50 Ω port.

In Figure 6b, the scattering S11 of the feeding signal at the input of ports p1 and p2, considering port impedance 50 Ω, is depicted. It is just an indicative result, which along with the input impedance (Figure 6a) is used to check if the antenna's performance has changed compared with Antenna_1.

A differentiation is observed. However, given that at the rectenna, the feeding ports will be removed and the circuitry of a matching network (MN) followed by the rectifier will be connected at the position of each one of them, what is substantially important is to effectively conjugate match the input impedance shown in Figure 6a to the input impedance of this circuitry, which is not 50 Ω. So, the next tasks are to select the rectifiers' type and also the frequency band or bands from which the rectenna will harvest energy. The latter depends on the application, namely the location at which the rectenna will be used. For this purpose, it is common practice, measurements to be received in the environment, with the intention to find out the frequencies of the existing RF signals with the highest power level. These are the ones that define the frequency 'window' or 'windows' of the MN or the MNs that will be designed. These steps are valid in case the antenna is a wideband, as with the one proposed in this work. If the antenna has one or more narrow bands of operation which do not match those found by measurements, it is necessary to redesign the antenna. In case the rectenna or rectennas will be fed wirelessly by man-made radiating systems, of course all three parts—radiating systems, rectennas' antennas, and MNs—will be designed at the same frequency bands.

The results presented in the following section, at first, were received using a simple full wave rectifier with a 'smoothing' circuit, namely a capacitor in parallel with resistance, connected at its output. It is well known that a rectenna's antenna, as more generally it is valid for an antenna which works as receiver, plays the role of a voltage source for the load at which it transfers the power captured from the environment. In the equivalent electric circuits shown in Figure 7a,b, V_{oc} is the antenna voltage induced at the open circuited antenna input terminals, Z_{in} is the complex input impedance of the antenna and Z_L, in the case of a rectenna, is the impedance shown at the input terminals of the full wave rectifier connected at its output with a resistive load R_o in parallel with a smoothing capacitance C_o. The power transferred from the antenna to the load, the DC obtained voltage, V_{DC}, at the output of the rectifier and the power, P_{in_rec} available at the input of the rectifier, depend on all the above parameters.

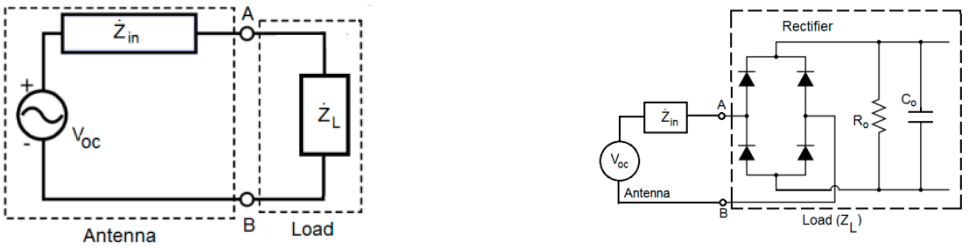

Figure 7. The equivalent circuitry of the antenna connected directly to the rectifier: (**a**) the equivalent loop circuit and (**b**) the details of the full wave rectifier with the resistance R_o and the smoothing capacitor C_o at its output.

For the full-wave rectifier, the Schottky diode HSMS-285C [26] (Broadcom Inc., San Jose, CA, USA) was considered. Its equivalent circuit includes a resistor of 3240 Ω in parallel with a capacitance of $C_D = 0.88$ pF. For the smoothing circuitry elements $C_o = 1$ nF and $R_o = 10$ KΩ, were used. This RC combination ensured very low, less than 0.01%, mean value of ripple, r, of V_{DC}, calculated as $r = 1/\left(4\sqrt{3}fR_oC_o\right)$.

Respecting the use of MN, although there is a tendency [27], in the case of rectennas, for such a network not to be used, due to power loss it inserts, in the present work results were received without MN and, for comparison, with MN. As the designed antenna holds its features of operation almost within the entire range of both frequency bands, two examples were elaborated. At one of them the target was a dual band operation to be obtained, namely at 920 MHz to 960 MHz, and around 1.8 GHz. The frequency ranges were selected because they are used as downlink bands at urban mobile telecommunication networks. The second example concerns a single band, at 868 MHz which is the

frequency of LoRA in Europe. For this purpose two different matching networks were synthesized applying the corresponding theory [28]. One of them is the dual band matcher, termed M-Net_1, shown in Figure 8a and the other is a single band one, termed as M-Net_2 and is depicted in Figure 8b. The values of the matching circuits' elements are included in Table 3.

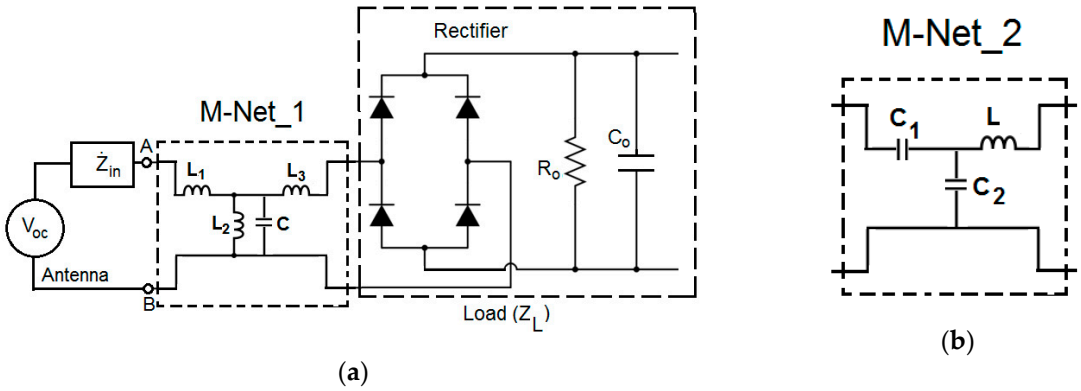

Figure 8. (**a**) The entire circuit of the antenna's equivalent circuit connected to the rectifier through the M-Net_1 and (**b**) the M-Net_2.

Table 3. The elements' values of M-Nets.

	M-Net_1		**M-Net_2**
L_1	22 nH	C_1	8.2 pF
L_2	10 nH	C_2	3.3 pF
L_3	18 nH	L	39 nF
C	1 pF		

3. Results and Discussion

3.1. Simulation and Calculation Steps

The available voltage and power at the input of the rectifier were termed respectively as V_{in_rec} and P_{in_rec} and the resulting DC voltage, V_{DC}, at its output depend, besides the effectiveness of the MN, on the power of the RF waves impinging to the antenna, on their DoAs, and also on the frequency. This performance is due to the fact that the Gain of the antenna depends also on DoAs and frequency and, in turn, these parameters of the incoming signals affect directly the V_{oc} magnitude [29]. Given that the waves arrive to the antenna from random directions, to make an assessment about the capabilities of the rectenna, as realistically as possible, the aforementioned quantities were calculated for a large number of DoAs and then statistical results over the DoAs and the frequencies of the bands of operation of MNs were produced. All the results were received via simulations. The $V_{in\text{-}rec}$ and $P_{in\text{-}rec}$ could be calculated by various ways: (a) we could simulate the operation of the antenna to find the V_{oc} induced at its open-circuited input terminals, namely without the presence on the rectifier and the matcher, for every DoA of the incoming waves and then to continue by using these V_{oc} values and the relative theory of the circuitry of matcher and rectifier to find the $V_{in\text{-}rec}$ and $P_{in\text{-}rec}$ (b) we could find, via simulations, the Gain of the antenna towards various directions which correspond to the DoAs suggested for the incoming waves and then, applying the corresponding theory for the power captured by the antenna [29] and also the circuitry theory of rectifier and matcher, to find the $V_{in\text{-}rec}$ and $P_{in\text{-}rec}$ and (c) to calculate the quantities entirely and directly by simulation. We followed the third way. The electric elements of the matchers were inserted at the simulator. In detail, as inductors and capacitors were considered commercial microwave chip inductors and capacitors [30,31] and in order to incorporate them to the designed rectenna, for simulation, the feeding microstrip line of each bowtie was textured near the position of its removed port, as shown in Figure 9.

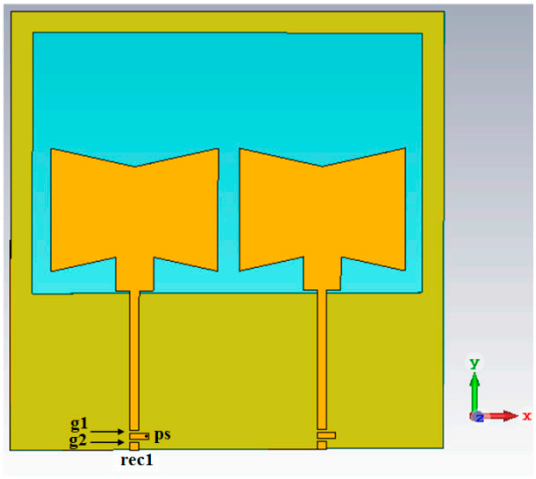

Figure 9. The layout of the rectenna and the positions at which the matching network (MN) elements and the rectifier were connected.

It is clarified that the values shown in Table 3 are the final ones and are a little different from those calculated by the mathematical formulae of the theory [28]. Changes were made for two reasons (a) they were necessary, as expected, with the intention that the simulations' results should agree with the theoretically selected frequencies of matching and (b) the commercial availability of the chip inductors and capacitors [30,31]. Moreover given that the considered RF chip capacitors and chip inductors are of ceramic type and have very low losses, the losses were not included in the calculations.

At gaps g1 and g2, the series-connected matcher elements were connected as lumped elements, while the shunt elements of the MNs were connected between the position ps (Figure 9) and the ground plane. At the end of the feeding line, namely the position of the removed port, the rectifier was inserted at the simulator (position rec1), by its equivalent circuit. This equivalent circuit was calculated taking into account the path of the current, at each alternating signal's period, that includes two diodes in series with the parallel combination of C_o and R_o. Given that the equivalent circuit of the used diodes is composed of a 3240 Ω resistor in parallel with a capacitance of $C_D = 0.88$ pF, the rectifier's equivalent circuit was calculated in terms of R, C elements which were inserted to the simulator. All the above are valid for the second bowtie, too. The quantities $V_{in\text{-}rec}$ and the power $P_{in\text{-}rec}$ available at the rectifier were calculated directly via simulation by suggesting plane waves incident to the rectenna from various DoAs. The quantity $V_{in\text{-}rec}$ was the simulated complex value of the voltage induced at the input of the rectifier and was being monitored, while the complex current $I_{in\text{-}rec}$ flowing through the rectifier was the second parameter that was also being monitored. The $P_{in\text{-}rec}$ was calculated as $P_{in\_rec} = \mathrm{Re}(\dot{V}_{in\_rec}\dot{I}^{*}_{in\_rec})$ and the DC voltage at the rectifier's output was calculated as $V_{DC} = \left|\dot{V}_{in-rec}\right|/\left(1 + r\sqrt{3}\right)$. An assessment for the power efficiency of the rectenna, was made by the ratio $n = P_{in\_rec}/P_{in\_ant}$, where P_{in_ant} is the power appearing at the input of the antenna namely the harvested power, and in accordance with the theory [29] it is calculated as $P_{in\_ant}(\theta, \varphi) = P_{inc}G(\theta, \varphi)\left(\lambda^2/4\pi\right)$ where P_{inc} is the power density of the wave impinging to the antenna, $G(\theta, \varphi)$ is the Realized Gain of the antenna at the direction (θ, φ) from which it accepts this power and λ is the wavelength. As P_{in_rec} is the power that arrives at the input of the rectifier, the index n substantially describes the portion of the harvested power that is delivered to the rectifier. The final DC power provided at the output of a full wave rectifier, as is well known, is about 81% of the power at its input, namely of the P_{in_rec}. So, applying the aforementioned steps, the required magnitudes were substantially received directly via simulation. We followed this method believing that it is the one more close to the physical process of harvesting the ambient RF power.

All the results presented were received considering, during the simulations, that the amplitude of the electric field intensity, of the circularly polarized incident waves, was E = 1.8 V/m. As mentioned previously, the variation of the antenna's characteristics versus frequency and also the dependence of

its gain on the direction in space, are impressed to V_{oc}, then to V_{in_rec} and finally to V_{DC}. So, in order to assess reliably the capabilities of the rectanna a statistical evaluation over these parameters was made.

The first part of the results presented in the following, includes the V_{DC} and P_{in_rec} in case of a matching network was not used and the equivalent circuit of the rectifier was connected directly to the antennas' inputs, namely at the position of the removed ports p1 and p2. The respective results, received when the MNs were connected, follow the first part.

3.2. Results without M-Nets

Figure 10a,b depict the variation, versus frequency, of V_{DC} and P_{in_rec}, indicatively for some DoAs of incoming waves. The directions are described by the angle θ and φ in space, measured from the axes -z- and -x- respectively. For example, θ = 0° and φ = 0° describe the DoA of a wave coming from the front side and impinging to the antenna perpendicularly to its plane, while θ = 180° and φ = 0° describe the DoA of a wave perpendicularly incident to the antenna, however impinging to its back side. As expected, the values of the voltage and power vary strongly by frequency and DoAs of the waves and this performance is due to the dependence of the antenna's Gain on the frequency and direction in space too, and it is ascertained by the Realized Gain graphs of Figure 11. At Figure 10a,b it is shown that although there is not any M-Net, a relatively satisfactory performance appears at two frequency regions. The lower one is in the UHF band, around 700 MHz and the higher, but with records less than in the lower, is between ~1.4 GHz and 1.6 GHz.

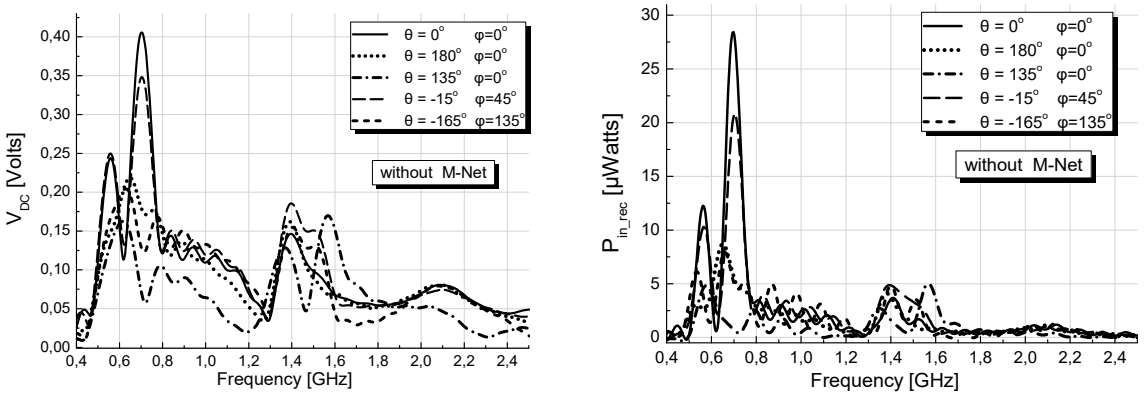

(**a**) (**b**)

Figure 10. Results versus frequency for rec1 without any M-Net: (**a**) direct current (DC) voltage at the output of the rectifier, (**b**) power available at the input of the rectifier.

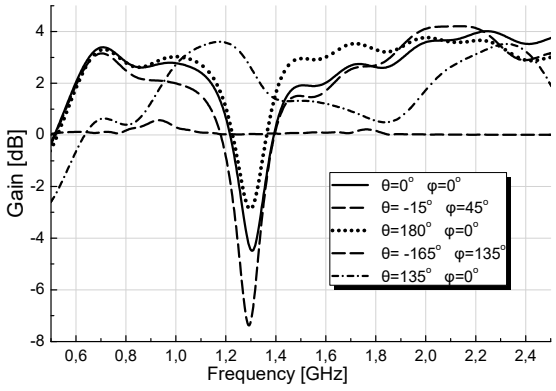

Figure 11. Antenna's Realized Gain versus frequency toward the directions of arrival (DoAs) of the previous results.

In the following subsections, results, indicatively, for two different cases at which a M-Net has been inserted between the antenna and the rectifier, are presented.

3.3. Results with M-Net_1

Figure 12a,b depict the variation, versus frequency, of V_{DC} at the output of the rectifier and the power P_{in_rec} available at its input, for DoAs of incoming waves similar to those of Figure 10a,b, for comparison purposes. As shown, the M-Net_1 obtains satisfactory matching between 920 MHz and 960 MHz and between ~1.72 GHz and 1.82 GHz, shifting the two frequency bands of good performance, shown in Figure 10, towards the selected higher frequencies and additionally enhancing the performance of the rectenna, as, satisfactory higher voltage and power values are obtained. This enhancement is more intense in the low band. At the high band the values of the magnitudes are not much larger than those received without matcher between ~1.4 GHz and 1.6 GHz. For all that, the M-Net_1 improves the performance in the high band, obtaining to ensure the same levels of voltage and power, for all the DoAs of the incoming signals. In contrast, when a MN is not used, there is high spread of voltage and power values with respect of DoAs, between 1.4 GHz and 1.6 GHz, as shown in Figure 10b.

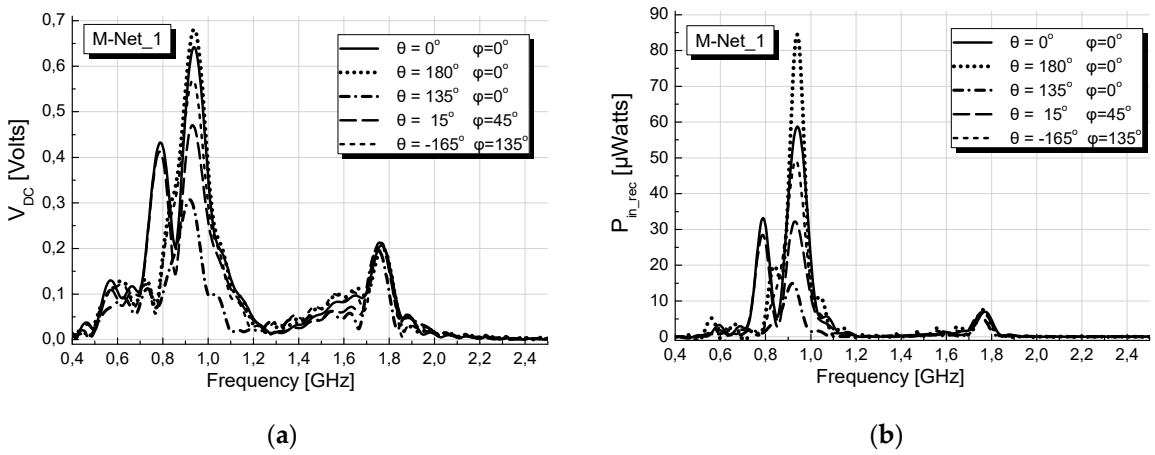

Figure 12. Results versus frequency when M-Net_1 is connected: (**a**) DC voltage at the output of the rectifier(rec1), (**b**) power available at the input of the rectifier.

It is also verified that the designed antenna can effectively harvest power from signals incident from both the front and the back space of its plane and it is due to the aperture created to the ground plane which in turn leads to radiation patterns presented in Figures 13 and 14. In these Figures the 3D Gain patterns of the antenna, when its elements are fed separately, are depicted, indicatively at one frequency inside the low and one at the upper band. In each case the front and back side of the patterns are shown. The results are in agreement with those of voltages and power and verify the capability of the antenna to effectively gather power from signals coming from both half spaces with respect to its plane. It is also observed that the radiation patterns, due to the symmetrical position of the two bowties mirroring each other, and the same observation is valid for the values of V_{DC} and P_{in_rec}. So, the voltage and power which appear to the rectifier of one of the elements for a specific DoA, appears also to the rectifier of the other element when the wave arrives from the mirrored DoA. That is why in Figures 10 and 12, results only for the rec1 are presented, while at the statistical results, which follow for the assessment of the overall rectenna's performance, results from both rectifiers were included.

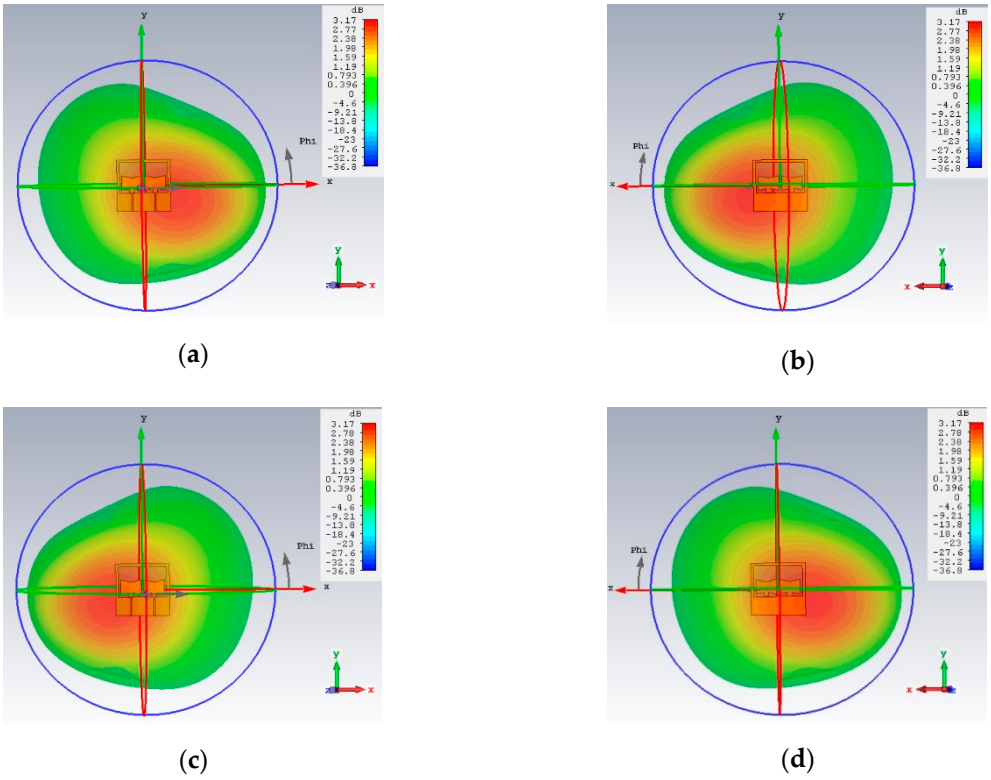

(**a**) (**b**)

(**c**) (**d**)

Figure 13. 3D Realized Gain patterns in the middle of the low frequency band (937 MHz): (**a**,**b**) in front of and back of the antenna plane (port p1 is fed), (**c**,**d**) respective results when port p2 is fed.

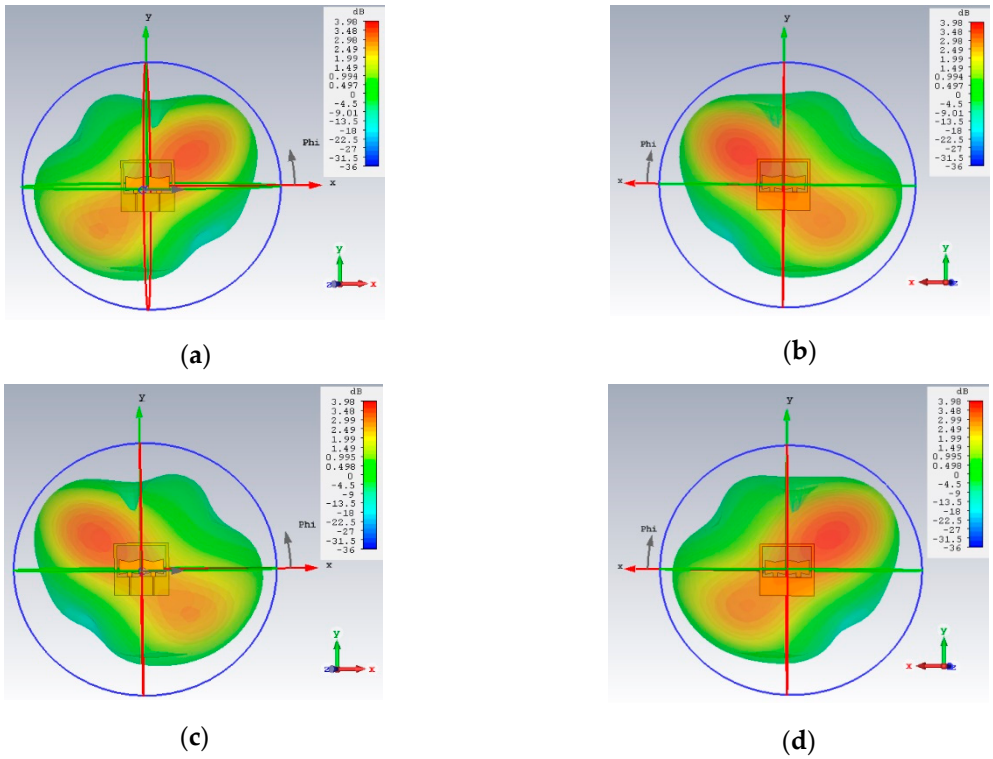

(**a**) (**b**)

(**c**) (**d**)

Figure 14. 3D Realized Gain patterns in the high frequency band (1.78 GHz): (**a**,**b**) in front of and back of the antenna plane (port p1 is fed), (**c**,**d**) respective results feeding port p2.

Figure 15a,b depict the box charts for V_{DC} and P_{in_rec} received for waves incoming from seven different DoAs within a region ±45° around -z- axis form the front side of the antenna and correspondingly from the back side. For comparison, results with and without M-Net are illustrated. The statistics were made over a total of 14 directions, the frequencies in the respective bands and for the rectifiers of both bowtie elements. The total statistical sample was 590 values at the lower band and 1490 values at the upper band. The records of the rectenna at the low band are as follows: the mean value of V_{DC} is 540 mV when M-Net_1 is used, while it is 112 mV without M-Net. The interquartile (IQR) range of the distribution, in the case of M-Net_1, extends from 455 mV (percentile 25%) to 625 mV (percentile 75%), while without M-Net the values are respectively 100 mV and 128 mV. Regarding the P_{in_rec}, with the M-Net_1, the mean value is 47 μW and the IQR range extends from 33 μW to 63 μW, while without M-Net the mean value is only 2 μW and the IQR range extends from ~1 μW to 3.5 μW. In this band, mean efficiency value n = 58.2% with the M-Net_1 is obtained while without MN, is very low, as expected, and equal to 5.4%.

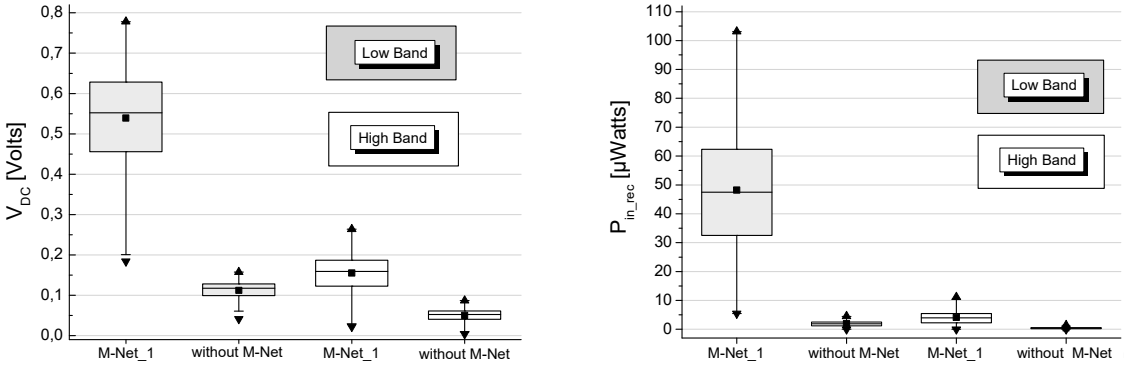

(**a**) (**b**)

Figure 15. With M-Net_1: statistical results over frequencies in the matching bands, the DoAs and both rectifiers for (**a**) V_{DC} (**b**) $P_{in\_rec.}$

Concerning the high band, the records of the rectenna are: the mean value of V_{DC} is 155 mV when M-Net_1 is used, and 50 mV without M-Net. The IQR range, in case of M-Net_1, extends from 125 mV to 180 mV, while without M-Net they are respectively 40 mV and 60 mV. Regarding the P_{in_rec}, with the M-Net_1, the mean value is 4 μW and the IQR range extends from 3 μW to 5 μW, while without M-Net all the values are around 1 μW. In this band the mean efficiency is n = 24.1% with the M-Net_1 and, again, very low (4.5%) without MN.

3.4. Results with M-Net_2

Figure 16a,b depict the variation, versus frequency for the voltage V_{DC} at the output of the rectifier 1 and the power P_{in_rec} available at its input, for DoAs of incoming waves similar to those of Figure 10a,b. As shown the M-Net_2 obtains satisfactory matching round 868 MHz.

It is verified that, at this frequency too, the designed antenna, can effectively harvest power from signals incident from both the front and the back space of its plane and the respective radiation patterns at 868 MHz are presented in Figure 17, leading to similar observations.

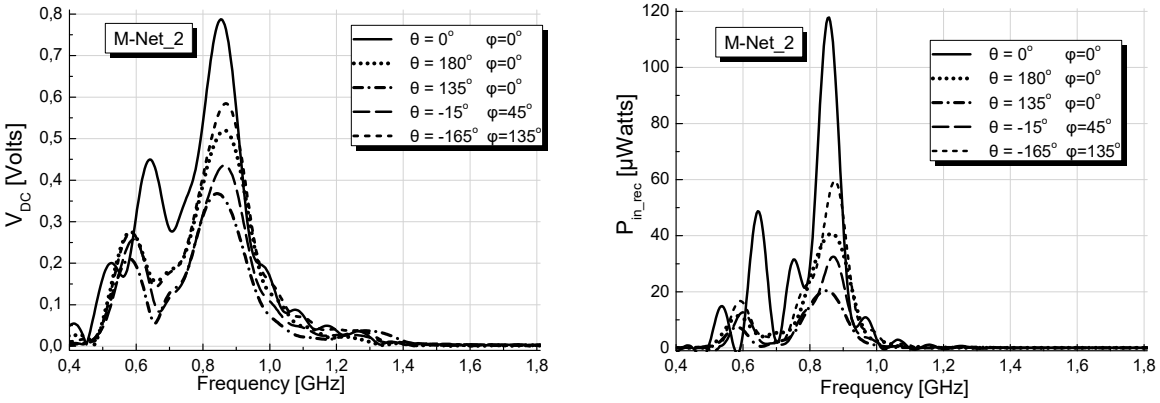

Figure 16. Results versus frequency when M-Net_2 is connected: (**a**) DC Voltage at the output of the rectifier (rec1) (**b**) power available at the input of the rectifier.

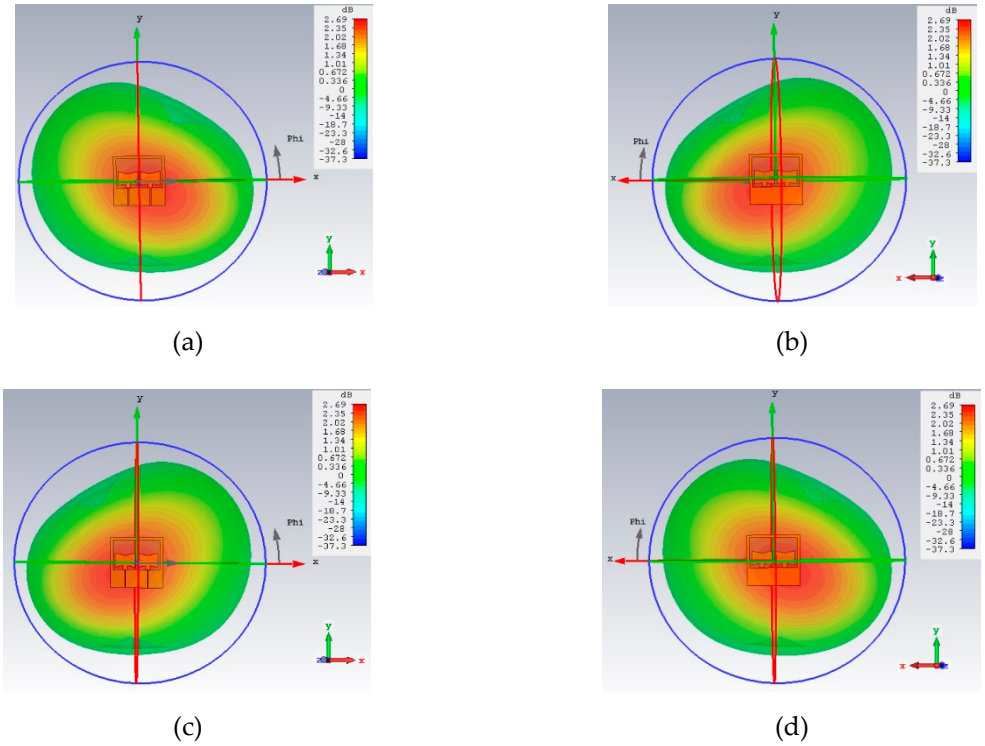

Figure 17. 3D Gain patterns at 868 MHz: (**a**) and (**b**) in front of and back of the antenna plane when port p1 is fed, (**c**) and (**d**) respective results when port p2 is fed.

Figure 18a,b were received with M-Net_2 and depict the box charts for V_{DC} and P_{in_rec}. The results were received for DoAs from the broadside and the backside of the antenna similarly to the results with the M-Net_1. The statistics were made over the total of 14 directions, with frequencies around 868 MHz and for the rectifiers of both bowtie elements, the statistical total being 594 samples. The records of the rectenna are: the mean value of V_{DC} is 580 mV with M-Net_2 and 120 mV without M-Net. The IQR range of the distribution, with the M-Net_2, extends from 500 mV to 700 mV and without M-Net from 112 mV to 127 mV. Regarding the P_{in_rec}, with the M-Net_2, the mean value is 58 μW and the IQR range extends from 35 μW to 78 μW, while without M-Net the mean value is 2.5 μW and the IQR range extends from ~2 μW to 3.5 μW. In this band the mean efficiency value is 68.3% with the M-Net_2 and, as expected, very low (4.1%) without MN.

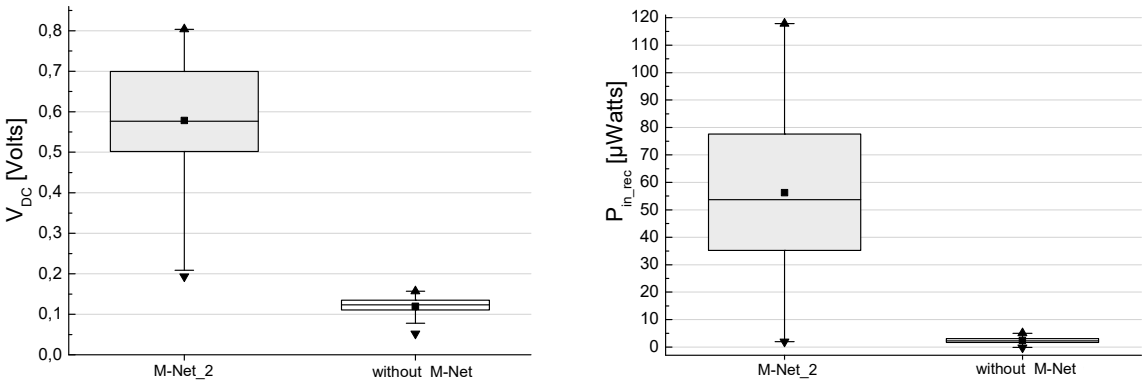

(**a**) (**b**)

Figure 18. With M-Net_2: statistical results over frequencies in the matching bands, the DoAs and both rectifiers for (**a**) V_{DC} (**b**) $P_{in\_rec.}$

4. Conclusions

In the paper, a preliminary study on analysis and design of a wideband array constituted of two patches of bowtie shape for an RF energy-harvesting application is proposed. The antenna array could be termed as a semi-printed radiator because although a ground plane exists, due to the aperture created to the ground behind the bowtie elements, they are not substantially microstrip but just printed radiators. The designed antenna is capable of receiving signals coming from its front side and equally from its back side and when connected with a simple full-wave rectifier through a matching network, properly designed to operate inside the antenna's bands of operation, can give satisfactory high DC voltages and power. It is pointed out that due to the wideband performance of the antenna, we could use it for various frequency slots as long as we change the operation frequency of the matching network. The size of the rectenna is 138.6 mm × 138.6 mm × 1.74 mm and is judged satisfactorily small, compared to the relatively large wavelengths at the frequencies of operation in the UHF band, and very good efficiency is obtained.

Statistical results received for various DoAs of incoming, circularly polarized, waves with electric field intensity amplitude 1.8 V/m, show that, with the matching network M-Net_1, within the low band, mean DC voltage value 540 mV and peak value 700 mV are obtained. Also with M-Net_1, in the high band the mean voltage is 155 mV and the peak voltage 275 mV. Using the M-Net_2, the mean voltage, around 868 MHz, is 580 mV and the peak voltage 800 mV. The mean values of the power available at the rectifier are respectively 47 μW, in the low band, 4 μW in the high band and 58 μW around 868 MHz. Correspondingly, the peak values are 100 μW, 12 μW and 120 μW. The mean values of the rectenna's efficiency, estimated by the ratio of the power available to the rectifier over the respective harvested by the antenna, are about 58%, 24% and 68% depending also on the MN and the frequency band. All the statistical mean and peak values with the presence of MNs are much higher than the respective ones without MNs. Moreover, these values concern each bowtie element and its rectifier separately. Thus, due to the antennas' geometry and the fact that inside the area occupied by the antenna, two elements exist and also two rectifiers, the entirely harvested amount of power is expected to be larger than that in case of one element. It is also pointed out that all the results were received considering only one plane wave incident to rectenna. However, in practice, more than one signal could arrive simultaneously at the elements of the antenna, coming from different directions and also having different power levels and in this way the gathered power would increase. On the other hand, the two elements do not harvest the same amount of power for each signal coming from a specific direction, either because they have different gain towards this direction, as the results show, and/or one of them would be prevented, by an obstacle to receiving a wave from this direction. Consequently, it is difficult a quantitative assessment about the increment of the harvested power to be done. Also, it is worth commenting that the polarization of the incoming waves was considered circular while the

bowties' polarization is linear and this fact inserts a decrease of about 50% to the gathered power and consequently to the received results. In other words if the polarization of the incoming waves was linear and was matched to the antenna's polarization, the harvested power would be greater but the study would not be realistic.

Author Contributions: Conceptualization, K.S. and A.K.; Formal analysis, K.S. and A.K.; Investigation, K.S. and A.K.; Methodology, K.S. and A.K.; Validation, K.S. and A.K.; Writing—original draft, K.S. and A.K.

Acknowledgments: The research has been co-financed by the European Union and Greek national funds through the Operational Program Competitiveness, Entrepreneurship and Innovation, under the call Research-CREATE-INNOVATE (project code: T1EDK-05274).

Conflicts of Interest: The authors declare no conflicts of interest.

References

1. Tan, Z.; Qu, H.; Zhao, J.; Ren, G.; Wang, W. Self-Sustainable Dense Cellular M2m System with Hybrid Energy Harvesting and High Sensitivity Rectenna. *IEEE Access* **2019**, *7*, 19447–19460. [CrossRef]
2. Ramesh, G.P.; Rajan, A. Microstrip Antenna Designs for RF Energy Harvesting. In Proceedings of the International Conference on Communication and Signal Processing (ICCSP 2014), Melmaruvathur, India, 3–5 April 2014; pp. 1653–1657.
3. Sun, H.; Guo, Y.-X.; He, M.; Zhong, Z. Design of a high-efficiency 2.45-GHz rectenna for low-input-power energy harvesting. *IEEE Antennas Wirel. Propag. Lett.* **2012**, *11*, 929–932.
4. Olgun, U.; Chen, C.-C.; Volakis, J.L. Investigation of rectenna array configurations for enhanced RF power harvesting. *IEEE Antennas Wirel. Propag. Lett.* **2011**, *10*, 262–265. [CrossRef]
5. Niotaki, K.; Kim, S.; Jeong, S.; Collado, A.; Georgiadis, A.; Tenzeris, M.M. A compact dual-band rectenna using slot-loaded dual band folded dipole antenna. *IEEE Antennas Wirel. Propag. Lett.* **2012**, *12*, 1634–1637. [CrossRef]
6. Palazzi, V.; Hester, J.; Bito, J.; Alimenti, F.; Kalialakis, C.; Collado, A.; Mezzanotte, P.; Georgiadis, A.; Roselli, L.; Tentzeris, M.M. A novel ultra-lightweight multiband rectenna on paper for RF energy harvestinG in the next generation LTE bands. *IEEE Trans. Microw. Theory Tech.* **2018**, *66*, 366–379. [CrossRef]
7. Mansour, M.M.; Kanaya, H. Novel L-Slot matching circuit integrated with circularly polarized rectenna for wireless energy harvesting. *Electronics* **2019**, *8*, 651. [CrossRef]
8. Yasuda, K.; Nishiyama, E.; Toyoda, I. A high efficiency differential rectenna employing two-parasitic-element stacked antenna. In Proceedings of the 2018 Asia-Pacific Microwave Conference (APMC-2018), Kyoto, Japan, 6–9 November 2018. WE2-C-4.
9. Shen, S.; Chiu, C.; Murch, R.D. A Dual-Port Triple-Band L-Probe Microstrip Patch Rectenna for Ambient RF Energy Harvesting. *IEEE Antennas Wirel. Propag. Lett.* **2018**, *16*, 3071–3074. [CrossRef]
10. Fantuzzi, M.; Masotti, D.; Costanzo, A. Rectenna array with RF-Uncoupled Closely-spaced Monopoles for Autonomous Localization. In Proceedings of the 48th European Microwave Conference (EuMA-2018), Madrid, Spain, 25–27 September 2018; pp. 765–768.
11. Kishimoto, H.; Itoh, K.; Noguchi, K.; Ida, J. Wideband rectenna with inductive high-impedance folded dipole antenna. In Proceedings of the IEEE Wireless Power Transfer Conference (WPTC-2018), Montreal, QC, Canada, 3–7 June 2018.
12. Okba, A.; Takacs, A.; Aubert, H. Compact rectennas for ultra-low-power wireless transmission applications. *IEEE Trans. Microw. Theory Tech.* **2019**, *67*, 1697–1707. [CrossRef]
13. Lu, P.; Huang, K.M.; Yang, Y.; Cheng, F.; Wu, L. Frequency-reconfigurable rectenna with an adaptive matching stub for microwave power transmission. *IEEE Antennas Wirel. Propag. Lett.* **2019**, *18*, 956–960. [CrossRef]
14. Polaiah, G.; Krishnamoorthy, K.; Kulkarni, M. Design of quatrefoil shape antennas for GSM1800 MHz and UMTS 2.1 GHz rectenna applications. In Proceedings of the URSI AP-RASC 2019, New Delhi, India, 9–15 March 2019.
15. Chen, Y.-S.; You, J.-W. A scalable and multidirectional rectenna system for RF energy harvesting. *IEEE Trans. Compon. Packag. Manuf. Technol.* **2018**, *8*, 2060–2072. [CrossRef]
16. Hu, Y.-Y.; Sun, S.; Xu, H.; Sun, H. Grid-array rectenna with wide angle coverage for effectively harvesting RF energy of low power density. *IEEE Trans. Microw. Theory Tech.* **2019**, *67*, 402–413. [CrossRef]

17. Li, X.; Yang, L.; Huang, L. Novel Design of 2.45-GHz Rectenna Element and Array for Wireless Power Transmission. *IEEE Access* **2019**, *7*, 28356–28362. [CrossRef]
18. Shen, S.; Chiu, C.; Murch, R.D. Multiport Pixel Rectenna for Ambient RF Energy Harvesting. *IEEE Trans. Antennas Propag.* **2018**, *66*, 644–656. [CrossRef]
19. Karampatea, A.; Siakavara, K. Analysis and synthesis of double negative dielectric media rectenna systems for ambient microwave energy harvesting. *Int. J. Antennas Propag.* **2018**, *2018*, 2472738. [CrossRef]
20. Karampatea, A.; Siakavara, K. Hybrid rectennas of printed dipole type on double negative dielectric media for powering sensors via RF ambient energy harvesting. *Int. J. Electron. Commun.* **2019**, *108*, 242–250. [CrossRef]
21. Cheng, Y.; Sheng, B. A printed bowtie dipole broadband directional antenna. In Proceedings of the 6th Asia-Pacific Conference on Antennas and Propagation (APCAP-2017), Xi'an, China, 16–19 October 2017.
22. Raut, S.; Petosa, A. A compact printed Bowtie antenna for ultra-wideband applications. In Proceedings of the 39th European Microwave Conference (EuMC-2009), Rome, Italy, 29 September–1 October 2009; pp. 81–84.
23. Basta, N.P.; Falkenstein, E.A.; Popovic, Z. Bow-Tie Rectenna Arrays. Proceeedings of the IEEE Wireless Power Transfer Conference (WPTC-2015), Boulder, CO, USA, 13–15 May 2015.
24. Kim, S.; Vyas, R.; Bito, J.; Niotaki, K.; Collado, A.; Georgiadis, A.; Tentzeris, M.M. Ambient RF energy-harvesting technologies for self-sustainable standalone wireless sensor platforms. *Proc. IEEE* **2014**, *102*, 1649–1666. [CrossRef]
25. Durgun, A.C.; Balanis, C.A.; Birtcher, C.R.; Alle, D.R. Design, simulation, fabrication and testing of flexible bow-tie antennas. *IEEE Trans. Antennas Propag.* **2011**, *59*, 4425–4434. [CrossRef]
26. Avago Technologies, Data Sheet HSMS-285x. Available online: https://pdf1.alldatasheet.com/datasheet-pdf/view/1072262/AVAGO/HSMS-285X.html (accessed on 23 January 2019).
27. Song, C.; Huang, Y.; Zhou, J.; Carter, P.; Yuan, S.; Xu, Q.; Fei, Z. Matching network elimination in broadband rectennas for high efficiency wireless power transfer and energy harvesting. *IEEE Trans. Ind. Electron.* **2017**, *64*, 1950–1961. [CrossRef]
28. Pozar, D.M. *Microwave Engineering*, 4th ed.; John Wiley & Sons: Hoboken, NJ, USA, 2012.
29. Balanis, C.A. *Antenna Theory: Analysis and Design*, 4th ed.; John Wiley & Sons: Hoboken, NJ, USA, 2016.
30. AVX-Advanced Electronic Components. Available online: https://www.avx.com (accessed on 23 January 2019).
31. Johanson Technology. Available online: https://www.johansontechnology.com (accessed on 23 January 2019).